

# Deriving the cosmic ray spectrum from gamma-ray observations

M. Kachelrieß<sup>1</sup> and S. Ostapchenko<sup>1,2</sup>

<sup>1</sup>*Institutt for fysikk, NTNU, Trondheim, Norway and*

<sup>2</sup>*D. V. Skobel'syn Institute of Nuclear Physics, Moscow State University, Moscow, Russia*

(Dated: May 24, 2012)

A fundamental problem of cosmic ray (CR) physics is the determination of the average properties of Galactic CRs outside the Solar system. Starting from COS-B data in the 1980's, gamma-ray observations of molecular clouds in the Gould Belt above the Galactic plane have been used to deduce the Galactic CR energy spectrum. We reconsider this problem in view of the improved precision of observational data which in turn require a more precise treatment of photon production in proton-proton scatterings. We show that the spectral shape  $dN/dp \propto p^{-2.85}$  of CR protons as determined by the PAMELA collaboration in the energy range  $80 \text{ GeV} < pc < 230 \text{ GeV}$  is consistent with the photon spectra from molecular clouds observed with Fermi-LAT down to photon energies  $E \sim 1\text{--}2 \text{ GeV}$ . Adding a break of the CR flux at  $3 \text{ GeV}$ , caused by a corresponding change of the diffusion coefficient, improves further the agreement in the energy range  $0.2\text{--}3 \text{ GeV}$ .

PACS numbers: 98.70.Sa, 13.60.Le, 98.38.Dq, 98.70.Rz

## I. INTRODUCTION

The propagation of cosmic ray (CR) protons and nuclei with energies  $E/Z \lesssim 10^{18} \text{ eV}$  in the turbulent component of the Galactic magnetic field resembles a random walk and can be described in general by the diffusion approximation [1]. Therefore the Galactic disk should be filled with a well-mixed “sea” of CRs whose properties are summarized by the differential diffuse intensity  $I(E)$  or the differential number density  $n(E) = 4\pi I(E)/v$ . Excluding the regions close to recent CR sources, the gradient  $\nabla \ln[n(E)]$  induced by the small current of CRs diffusing out of the disc and its extended CR halo is small.

Most of our knowledge about Galactic CRs is obtained via observations in our local environment. Despite of the diffusive propagation of CRs, the CR intensity deduced locally may differ from the one averaged over the Galactic disc: At low energies, the influence of the Solar wind on measurements of the CR energy spectrum and the total CR energy density has to be corrected based on current understanding of the heliospheric modulation and direct CR measurements at different heliospheric distances and at different modulation levels. Clearly, such a correction is model-dependent and can introduce uncertainties. Moreover, the Sun is close to a region with increased star-formation and thus supernova rate. Other reasons for local deviations include stochastic re-acceleration in the local interstellar turbulence or local sources as old supernova shocks, winds and flares of massive stars. Therefore, the CR density close to the Solar system may deviate from the average Galactic one.

A way to obtain independent information on the average “sea” Galactic CRs is the observation of suitable molecular clouds far from CR accelerating regions [2]: These clouds serve as a target for CRs producing gamma-rays mainly through decays of neutral pions created as secondaries in CR-gas collisions. Suitable clouds should be located away from the Galactic plane in order to test the “sea” CR spectrum, excluding the directions towards

the inner and outer Galaxy. Assuming that gamma-ray production in hadronic interactions is sufficiently well-understood, the observed gamma-ray flux  $\mathcal{F}_\gamma(E)$  from these clouds can be inverted to obtain the differential CR number density  $n(E)$ .

Previous works used observations of molecular clouds in the Gould Belt, in particular of Orion A and B, performed first by COS-B [3], then EGRET [4, 5], and most recently Fermi-LAT to derive the spectral shape of Galactic CRs. During this period, the quality of experimental data has been hugely improved: On the observational side, the data from Fermi-LAT have a much reduced error compared to its predecessor EGRET and extend now up to photon energies  $E_\gamma \sim 100 \text{ GeV}$ , corresponding to typical energies of CR primaries  $E \sim 1 \text{ TeV}$ . Moreover, the PAMELA collaboration determined the slope  $\beta_{\text{CR}}$  of the CR spectrum  $dN/dp \propto p^{-\beta_{\text{CR}}}$  with an accuracy of  $\Delta\beta_{\text{CR}} = \pm 0.05$  in the energy range  $80 \text{ GeV} < pc < 230 \text{ GeV}$  [6]. Thus the prediction of the secondary photon spectrum requires either similar precise photon fragmentation functions, or at least an estimate of their error. Finally, there are new results on photon yields from HERA [7] as well as from LHC [8] on the accelerator side, restricting theoretical models for photon fragmentation functions.

In view of the improved precision of the experimental data, we reconsider this problem, paying special attention to the treatment of photon production in proton-proton scatterings. We find that several commonly used parametrisations for the photon fragmentation function as the ones of Refs. [9, 10] deviate substantially from experimental data at high energies. These differences diminish considering the photon yield produced by CRs with a power-law momentum distribution. In this case, we find a relatively good agreement concerning the shape of the photon spectra, while the absolute photon yield differs by  $\sim 20\%$ . As our main result, we show that the spectral shape  $dN/dp \propto p^{-2.85}$  of CR protons as determined by PAMELA in the energy range  $80 \text{ GeV} < pc <$

230 GeV [6] is consistent with the photon spectra from molecular clouds observed by Fermi-LAT down to energies  $E \sim 1\text{--}2$  GeV. The agreement is further improved, if the CR spectrum exhibits a break around 3 GeV, as suggested by radio data [11].

This work is structured as follows: We compare first in Sec. II several models used for the calculation of photon production in hadronic collisions to experimental data. We conclude that a combination of the parametrization of Ref. [9] for nondiffractive processes below  $E_{\text{thr}} = 50$  GeV with the QGSJET-II model [12] at higher energies gives a satisfactory description of experimental data. Then we calculate in Sec. III the photon spectra expected from molecular clouds for a given CR flux. In the appendix, we describe the use of the photon and antiproton fragmentation functions employed by us which are available from <http://sourceforge.net/projects/ppfrag>.

## II. MODELS FOR PHOTON PRODUCTION

High-energy photons can be produced both by CR protons and electrons. In the latter case, inverse Compton scattering on photons mainly from the cosmic microwave background and bremsstrahlung are potentially contributing processes. In particular, bremsstrahlung was discussed as an important contribution to the total observed gamma-ray spectrum from molecular clouds at energies below 100 MeV [5]. In this work, we restrict ourselves however to the energy range  $E_\gamma > 200$  MeV observed by Fermi-LAT where bremsstrahlung can be neglected. For the density of molecular clouds, also inverse Compton scattering gives a negligible contribution relative to photon production in CR-gas collisions.

Photon production in hadronic collisions results mainly from decays of neutral pions produced as secondaries. At sufficiently high energies, an additional though much smaller contribution comes from  $\eta$  decays, while direct photon production is strongly suppressed and negligible for astrophysical applications<sup>1</sup>.

The photon yield in hadronic collisions can be calculated using either numerical parametrisations or Monte Carlo simulations. The former are typically based on theoretically motivated or empirical scaling laws fitted to accelerator data. In general, they are well-suited for collisions at relatively low energies  $E \lesssim 50$  GeV. In contrast, Monte Carlo simulations are developed mainly for high-energy collisions and are based on a combination of non-perturbative models and perturbative QCD. They treat both soft interactions and the hadronization of partons produced in (semi-) hard scattering processes.

<sup>1</sup> In contrast, the results of Ref. [13] seem to indicate a significant contribution from direct photon production. This surprising result is explained by the simple fact that the authors of Ref. [13] refer misleadingly to photons from  $\eta$  decays as direct photons.

	10 GeV	100 GeV	1 TeV	10 TeV	100 TeV
QGSJET-II-04	0.62	0.64	0.64	0.70	0.79
SIBYLL 2.1	-	0.71	0.84	0.93	1.1
Model of Ref. [9]	0.57	0.78	0.73	0.84	1.1
ND model of [9]	0.48	0.53	0.48	0.49	0.69

TABLE I: Predictions for the spectral-weighted moment  $Z_\gamma(E_0)$  (in mb) for photon production in  $pp$  collisions at different laboratory energies  $E_0$ : Comparison of QGSJET-II-04, SIBYLL 2.1, the parametrization of Ref. [9], and the non-diffractive (ND) model of Ref. [9]; all for  $\beta_{\text{CR}} = -2.85$ .

In the next subsection, we compare the results derived using the ‘‘Kamae’’ parametrisation for the photon fragmentation function given in Ref. [9] to those obtained from the Monte Carlo simulations with the QGSJET-II-04 [12] and SIBYLL 2.1 [14] models, the latter having been used as the basis for the parametrization of the photon fragmentation function of Ref. [10].

### A. Comparison of the Kamae parametrisation and QGSJET-II

We start by recalling some basic analytical formula before we discuss our numerical results for the various quantities characterizing photon production in hadronic collisions. Assuming a power-law cosmic ray spectrum,  $dN_{\text{CR}}/dE = N_0 E^{-\beta_{\text{CR}}}$ , the resulting  $\gamma$ -ray flux may be written as

$$\begin{aligned} \frac{E_\gamma^2 dN_\gamma}{dE_\gamma} &\propto E_\gamma^2 \int_{E_\gamma}^{E_{\text{max}}} dE' \frac{dN_{\text{CR}}}{dE'} \frac{d\sigma^{pp \rightarrow \gamma}(E', E_\gamma)}{dE_\gamma} \\ &\propto E_\gamma^{2-\beta_{\text{CR}}} \int_0^1 dx_E \frac{x_E^{\beta_{\text{CR}}-1} d\sigma^{pp \rightarrow \gamma}(E_\gamma/x_E, x_E)}{dx_E} \\ &\equiv E_\gamma^{2-\beta_{\text{CR}}} \tilde{Z}_\gamma(E_\gamma), \end{aligned} \quad (1)$$

where  $x_E = E_\gamma/E'$  and we have assumed  $E_{\text{max}} \gg E_\gamma$ . Thus, any difference in the spectral shape between the parent CRs and the produced photons is introduced by the violation of Feynman scaling, i.e. by the energy dependence of the spectral moment  $\tilde{Z}_\gamma$ . Such a dependence emerges because of i) the slow energy rise of the inelastic  $pp$  cross section  $\sigma_{pp}^{\text{inel}}(E)$ , ii) the relatively fast increase of the central rapidity plateau of secondary particles  $1/\sigma_{pp}^{\text{inel}} d\sigma_{pp}^{\pi^0(\eta)}/dy|_{y=0}$ , and iii) the slow ‘‘softening’’ of the forward spectra of secondary mesons. While the first two effects result in an energy rise of  $\tilde{Z}_\gamma$ , the third one works in the opposite direction.

For our purposes, it is more convenient to consider moments  $Z_\gamma(E_0)$  defined for a given energy  $E_0$  of the CR proton in the  $pp$  collision,

$$Z_\gamma(E_0) = \int_0^1 dx_E \frac{x_E^{\beta_{\text{CR}}-1} d\sigma^{pp \rightarrow \gamma}(E_0, x_E)}{dx_E}. \quad (2)$$

In Table I, we illustrate the energy dependence of  $Z_\gamma(E_0)$ ,

using  $\beta_{\text{CR}} = -2.85$  as reported by the Pamela Collaboration in the range  $50 \text{ GeV} < E_0 < 200 \text{ GeV}$  [6], comparing the predictions of the QGSJET-II-04 [12] and SIBYLL 2.1 [14] Monte Carlo generators to the results obtained using the parametrization of  $d\sigma^{pp \rightarrow \gamma}(E_0, E_\gamma)/dE_\gamma$  from Ref. [9]. Clearly, the considered models predict a quite different behavior of  $Z_\gamma(E_0)$  in the energy range of interest: While in the case of QGSJET-II the spectral moment is approximately energy-independent up to  $E_0 \sim 1 \text{ TeV}$ ,  $Z_\gamma(E_0)$  has a relatively steep energy rise in the other two models.

In order to decide which of these approaches provides a better description of photon production, we compare them next to data from accelerator experiments. We start by considering the respective results for photon spectra in proton-proton collisions at  $205 \text{ GeV/c}$  laboratory momentum in Fig. 1 and for spectra of neutral pions and etas in  $pp$  collisions at  $p_{\text{lab}} = 250$  and  $400 \text{ GeV/c}$  in Figs. 2 and 3. In the case of QGSJET-II, the comparison demonstrates a good overall agreement between the predictions and the experimental data. The Feynman  $x_F$  spectra of photons and neutral pions obtained with SIBYLL 2.1 are very similar to the QGSJET-II case at small  $x_F$ , but become substantially harder with increasing energy for  $x_F \gtrsim 0.2$ , see Figs. 1–4.

As the accuracy of the fixed-target data considered does not allow one to discriminate between these two trends, a valuable benchmark is provided by recent HERA measurements of photon production in the proton fragmentation region for  $p\gamma^*$  interaction at  $\sqrt{s} = 319 \text{ GeV}$  [7]: The observed forward energy spectra of gammas appear to be well-described by QGSJET-II, while being substantially softer than SIBYLL predictions.

At first sight, this conclusion seems to be in a contradiction with the results of spectrometer studies of  $pp$  collisions at  $\sqrt{s} = 7 \text{ TeV}$  by the LHCf collaboration [8]: The measured very forward photon spectra proved to be significantly harder than predicted by QGSJET-II. However, the preliminary results on the  $\pi^0$  production at  $\sqrt{s} = 7 \text{ TeV}$  by the same collaboration indicate that the latter discrepancy is likely due to a somewhat softer than observed transverse momentum distribution of neutral pions in QGSJET-II [15]<sup>2</sup>. The latter conjecture is supported also by the HERA data of Ref. [7] which demonstrate that the  $p_t$ -spectra of forward photons are better described by SIBYLL 2.1 than by QGSJET-II. We conclude that QGSJET-II agrees well with the experimental data on the energy spectra of photons. The predicted  $p_t$  distributions are somewhat too soft, but are anyway irrelevant for our problem.

Though the considered Monte Carlo simulations are not designed to treat hadronic collisions for  $E_0 \lesssim 50$

GeV, the QGSJET-II results appear to be relatively reasonable down to  $\sim 12 \text{ GeV/c}$  laboratory momentum, as demonstrated in Fig. 5. However, extrapolating the model to even smaller energies is meaningless, because the relevant physical processes, like resonance production and secondary Reggeon exchanges, are not included. Indeed, as it can be clearly seen in Fig. 6, at  $8.8 \text{ GeV/c}$  laboratory momentum QGSJET-II tends to predict a harder photon spectrum than observed experimentally.

In contrast, the situation with the model of Ref. [9] appears to be quite different: This parametrization describes the experimental data quite well up to  $E_0 \sim 10 \text{ GeV}$ , cf. Figs. 5 and 6. Figures 1 and 4 show that the photon spectra predicted by the Kamae parametrization become at higher energies much harder than those of QGSJET-II which, as we have argued above, agree with HERA data. This explains the larger values for  $Z_\gamma(E_0)$  obtained in that case in the energy range  $E_0 \gtrsim 100 \text{ GeV}$ , see Table 1. The discrepancy between the parametrization of Ref. [9] and the data has its origin in the somewhat oversimplified treatment of diffractive particle production in the underlying model [16] which utilises a cluster-like hadronization procedure: The energy of the diffractive state is distributed more or less uniformly between the pions produced, neglecting the leading baryon effect. In reality, a large part of high energy diffraction corresponds to the creation of high mass states which are described by the Pomeron contribution and correspond to multiperipheral kinematics of particle production<sup>3</sup> [17]. As a consequence, forward spectra of neutral pions and etas in high mass diffractive processes resemble the ones of the usual nondiffractive collisions.

The complementarity of the two models motivated us to combine the QGSJET-II description with the parametrization of Ref. [9]: While we use QGSJET-II for photon production at relatively high energies  $E_0 > E_{\text{thr}}$ , with  $10 \lesssim E_{\text{thr}} \lesssim 50 \text{ GeV}$ , at lower energies we apply the parametrization of Ref. [9] restricted to *nondiffractive* processes.

### III. GAMMA-RAY SPECTRA

We explore now the consequences of our new photon fragmentation function. Let us remind first that diffusive shock acceleration predicts a power-law in momentum,  $dN/dp \propto p^{-\beta_{\text{CR}}}$ , cf. Ref. [19], while the interstellar propagation is also rigidity-dependent. It is, therefore, natural to use a power-law in rigidity to fit CR data. Indeed, PAMELA p and He spectra and their ratio can be well-described with a power-law in rigidity down to  $\sim 20 \text{ GV}$ , below which the interstellar spectrum is significantly modified by the heliospheric modulation.

<sup>2</sup> Fixed angle spectrometer measurements of forward particle spectra are very sensitive both to the respective Feynman  $x$  and  $p_t$  distributions, the two variables being related to each other in the c.m. frame as  $p_t = \vartheta_{\text{obs}} x_F \sqrt{s}/2$ .

<sup>3</sup> Even more complicated diffractive final states are produced at much higher energies [12, 18].

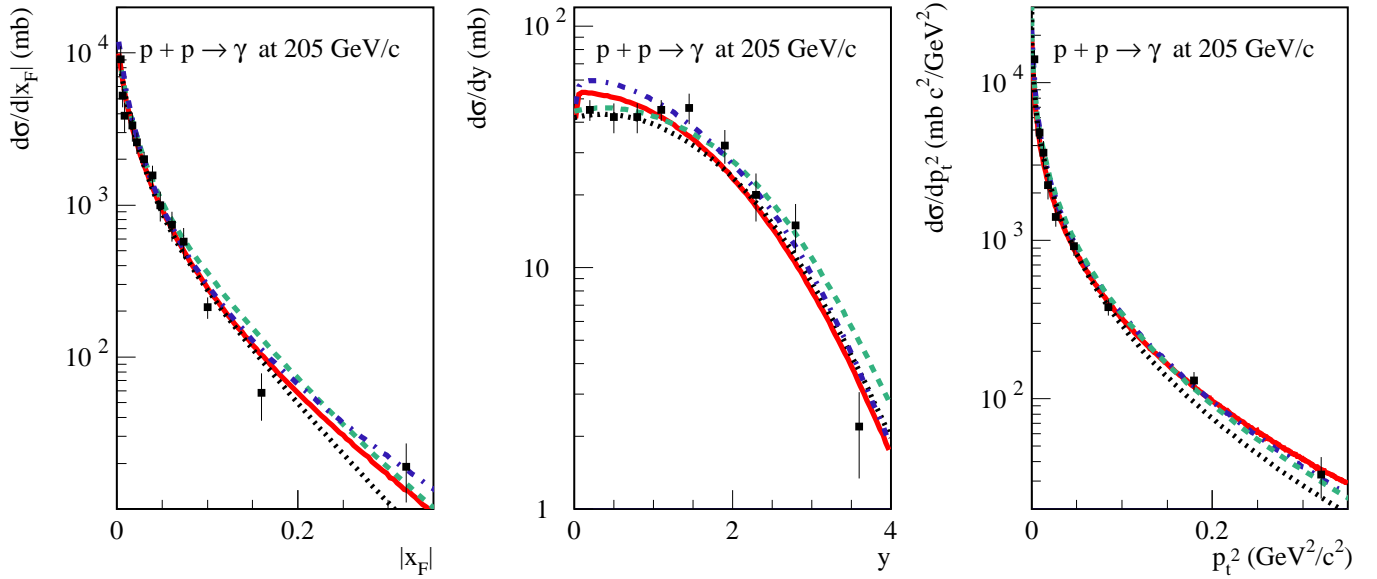


FIG. 1: Photon production cross sections in the center of mass (c.m.) frame for proton-proton collisions at 205 GeV/c: Feynman  $x$  spectrum (left), rapidity distribution (middle), and transverse momentum distribution (right). Calculations with QGSJET-II-04 (red solid), SIBYLL 2.1 (blue dot-dashed), parametrization of Ref. [9] (green dashed), and ND part (black dotted line) of the latter are shown together with experimental data from Ref. [21].

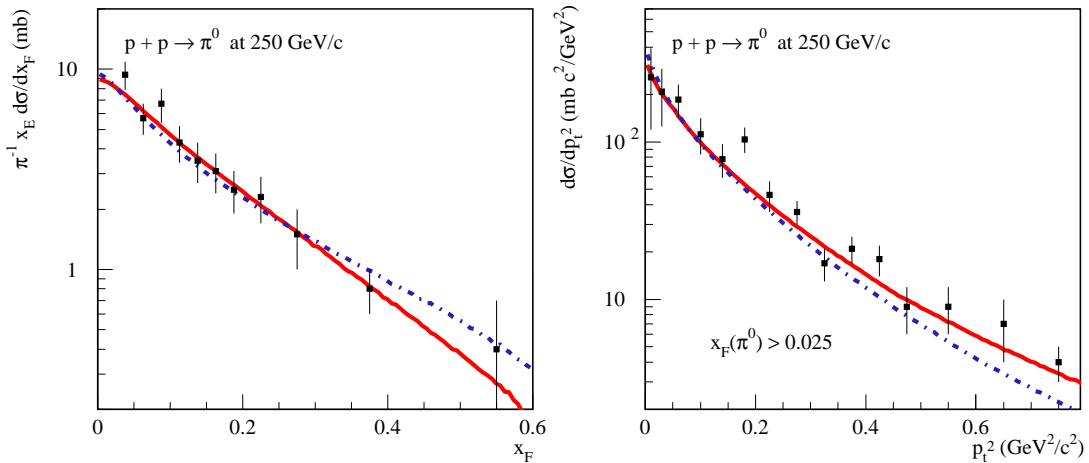


FIG. 2: Feynman  $x$  spectrum (left) and transverse momentum distribution (right) of neutral pions in the c.m. frame for  $pp$  collisions at 250 GeV/c as calculated using QGSJET-II-04 (red solid) and SIBYLL 2.1 (blue dot-dashed) compared to the data from Ref. [22].

In Fig. 7, we compare the gamma-ray spectrum produced by cosmic rays with  $dN/dp \propto p^{-2}$  using QGSJET-II, the parametrization of Ref. [9], or using only the nondiffractive part of the latter. The photon spectrum obtained using the Kamae parametrization rises much quicker with energy in the 1–10 GeV range than the one obtained with QGSJET-II, as a result how the diffraction is modeled in Ref. [16], while at higher energies the obtained spectra have similar shapes, with  $\sim 20\%$  difference in the normalization. On the other hand, the results obtained using the nondiffractive part of the Kamae parametrization agree well with QGSJET-II up to

few tens of GeV – compatible with the similarity of the photon spectra for  $pp$  collisions in the two models in the energy range  $E_p \sim 10 - 200$  GeV seen<sup>4</sup> in Figs. 1 and 4. Therefore, we find it natural to match in the following the results of the QGSJET-II model for photon spectra to the parametrization of Ref. [9] for nondiffractive processes at  $E_{\text{thr}} = 50$  GeV.

---

<sup>4</sup> The difference at 1–3 GeV is caused by the extrapolation of the QGSJET-II model outside its working range: Below 10 GeV lab. energy, it predicts too hard photon spectra, as shown in Fig. 6.

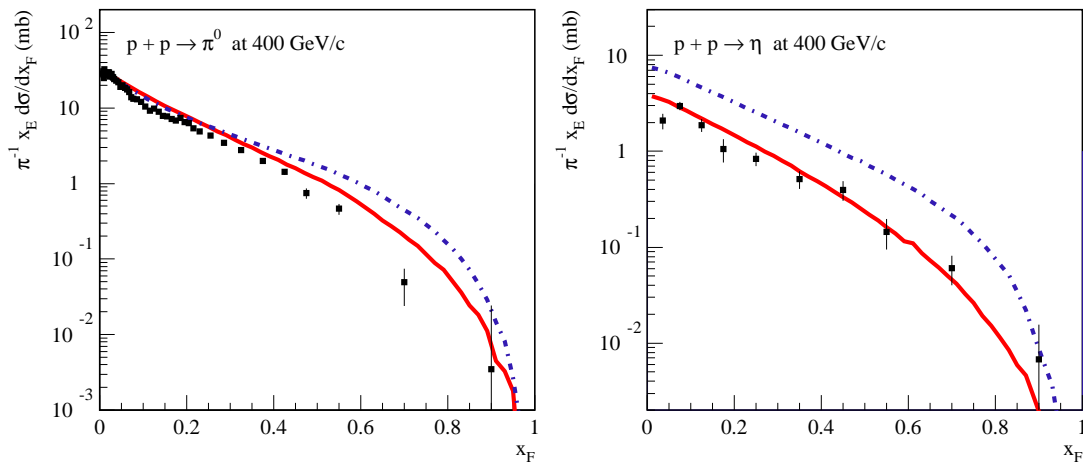


FIG. 3: Feynman  $x$  spectra for  $\pi^0$  (left) and  $\eta$  (right) production in the c.m. frame for  $pp$  collisions at 400 GeV/c as calculated using QGSJET-II-04 (solid) and SIBYLL 2.1 (dot-dashed) compared to the data from Ref. [23].

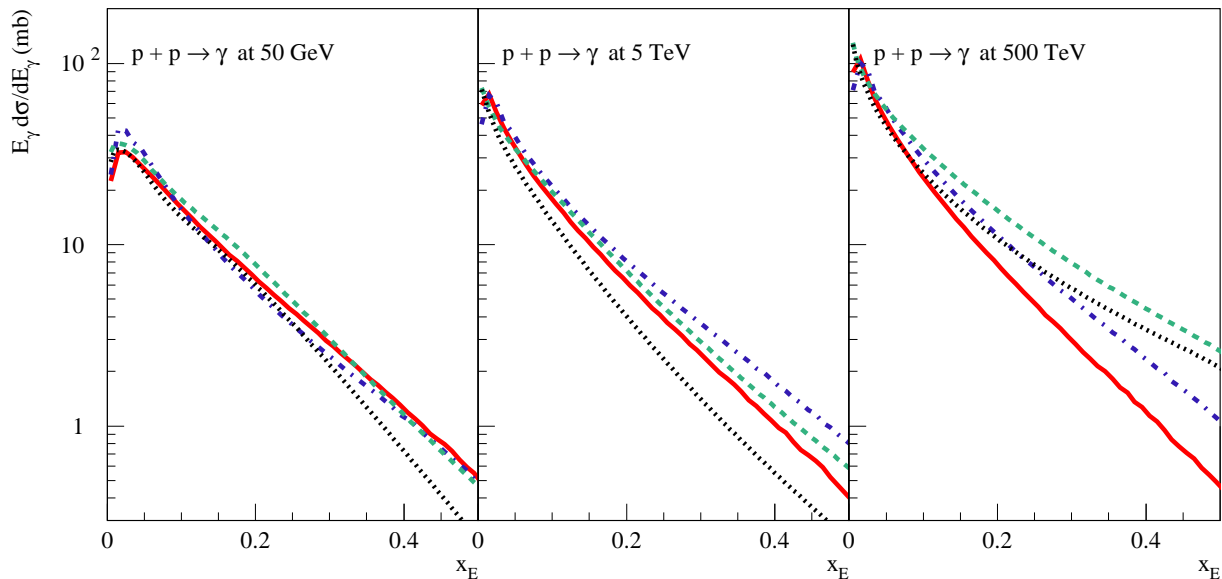


FIG. 4: Calculated energy distributions of photons in the laboratory frame for  $pp$  collisions at 50 GeV, 5 TeV, and 500 TeV; abbreviations for the lines are the same as in Fig. 1.

As a further application of our new photon fragmentation functions, we consider the problem how the cosmic ray spectrum can be derived from gamma-ray observations. The Fermi LAT collaboration has studied this question in great detail and using a variety of methods [28–31]: For instance, the diffuse Galactic gamma-ray emission was compared in Ref. [28] to GALPROP models and an overall agreement of  $\sim 15\%$  of data and models was found. In Ref. [29], the analysis of the diffuse gamma-ray emissivity was constrained to well-defined segments of the Local and the Perseus arms, deriving thereby constraints on the cosmic ray density gradient. Using observations in the mid-latitude region in the third quadrant, the Fermi-LAT collaboration concluded in Ref. [30] that the CR spectrum derived agrees

with the locally measured one within 10%.

More recently, the authors of Ref. [32] used Fermi-LAT observations of nearby molecular clouds to deduce the energy spectrum of Galactic sea CRs. The photon flux deduced in Ref. [32] is shown in Fig. 8 as red error-bars together with the photon spectrum (dashed green line) derived by us assuming a cosmic ray spectrum characterized by the slope  $\beta_{\text{CR}} = -2.85$ , and using the combination of QGSJET-II results for  $E_p > 50$  GeV with the parametrization of Ref. [9] for nondiffractive processes at lower energies. The predicted photon flux agrees well with the data at energies  $E_\gamma \gtrsim 1$  GeV. The remaining discrepancy at lower energies is at most at 30% level and may be partly related to uncertainties in the description of photon production at  $E_0 \lesssim 50$  GeV [9]. A more im-

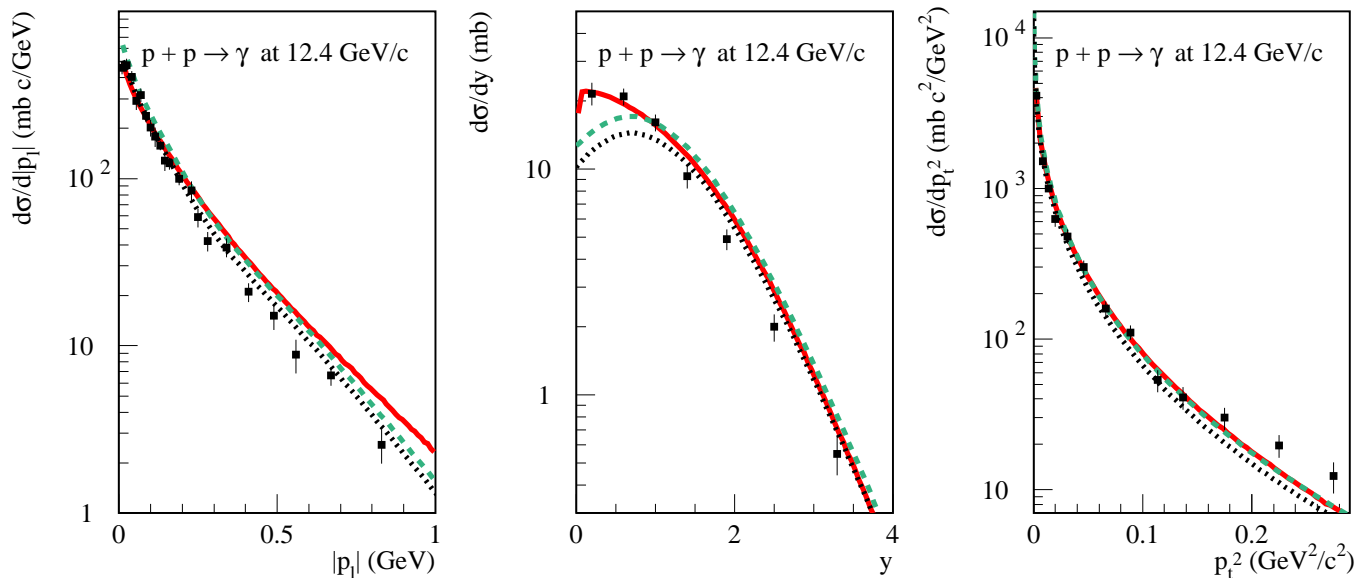


FIG. 5: Longitudinal momentum spectrum (left), rapidity distribution (middle), and transverse momentum distribution (right) of photons in the c.m. frame for  $pp$  collisions at 12.4 GeV/c as calculated using QGSJET-II-04 (solid lines) compared to experimental data from Ref. [24]. Dashed and dot-dashed lines - parametrizations of Ref. [9] for photon production in inelastic and nondiffractive  $pp$  collisions, respectively.

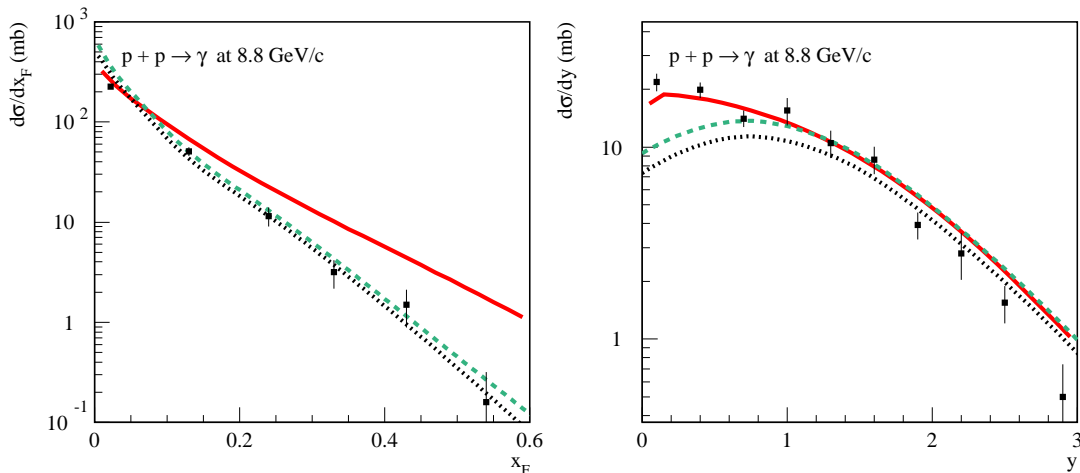


FIG. 6: Calculated Feynman  $x$  (left) and rapidity (right) spectra of photons in the c.m. frame for  $pp$  collisions at 8.8 GeV/c compared to experimental data from Ref. [25]; abbreviations for the lines are the same as in Fig. 5.

portant reason for the difference at energies  $E_\gamma \lesssim 1$  GeV may be the energy-dependence of the diffusion coefficient, which is expected to change at 2–3 GeV [11, 20]: For instance, Ref. [11] found fitting Galactic synchrotron data that the diffusion coefficient reaches a minimum at 2–3 GeV, increasing as  $p^{-1}$  or even faster at lower momenta  $p$ . To illustrate the latter point, we calculated the diffuse gamma-ray flux for the case of a broken power-law CR spectrum: with the slope  $\beta_{\text{CR}} = -2.85$  for  $p_{\text{CR}} > 3$  GeV/c and  $\beta_{\text{CR}} = -1$  for  $p_{\text{CR}} < 3$  GeV/c. The result, plotted in Fig. 8 as the solid blue line, matches well the observations in the whole energy range considered.

Next we examine, if a spectral break at higher energies is also consistent with the Fermi-LAT data. In particular, a broken power-law with high-energy slope  $\beta_{\text{CR}} \simeq -3$ , low-energy slope  $\beta_{\text{CR}} \simeq -1.9$ , and break-energy at  $T = E_p - m = 9$  GeV, or  $E_p \simeq 10$  GeV, has been obtained in Ref. [32] as best-fit to the Fermi-LAT data. In Fig. 9, we show as blue solid line the gamma-ray flux corresponding to a CR spectrum with the slope  $\beta_{\text{CR}} = -3$  for  $p_{\text{CR}} > 10$  GeV/c and  $\beta_{\text{CR}} = -2.4$  for  $p_{\text{CR}} < 10$  GeV/c which agrees clearly with the data also well. Note that the sharper spectral break obtained in Ref. [32], with the slope  $\beta_{\text{CR}} = -1.9$  for  $T < 9$  GeV, is caused by the use of the power-law CR spectra with

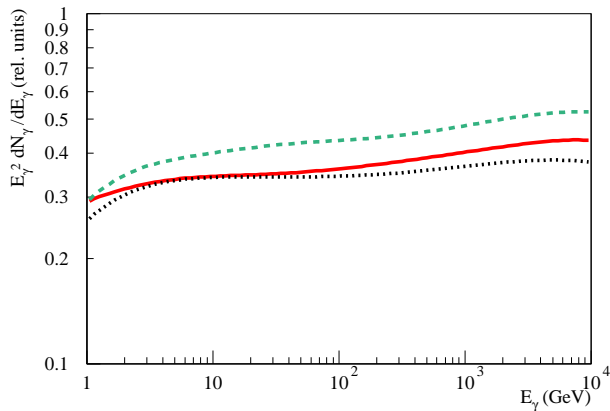


FIG. 7: Gamma-ray flux  $E^2\mathcal{F}(E)$  produced by cosmic ray protons with a spectrum  $dN/dp \propto p^{-2}$  as calculated using QGSJET-II (solid red line), the Kamae parametrization [9] (dashed green line), or the nondiffractive part of the latter (dotted black line).

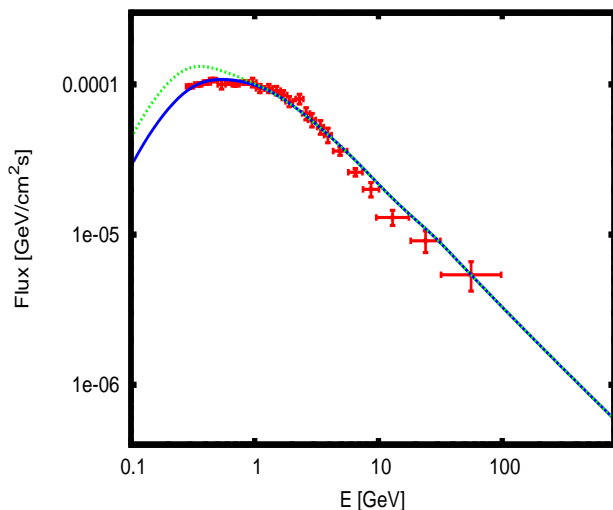


FIG. 8: Gamma-ray flux  $E^2\mathcal{F}(E)$  as calculated using the combination of QGSJET-II and the ND model of Ref. [9] ( $E_{\text{thr}} = 50$  GeV) for a single power-law CR flux with the slope  $\beta_{\text{CR}} = -2.85$  (dashed green line) and for a broken power-law with  $\beta_{\text{CR}} = -2.85$  for  $p_{\text{CR}} > 3$  GeV/c and  $\beta_{\text{CR}} = -1$  for  $p_{\text{CR}} < 3$  GeV/c (solid blue line). The gamma-ray spectrum derived in Ref. [32] from Fermi-LAT data is shown as points with error-bars.

respect to the kinetic energy in Ref. [32], leading to a substantial enhancement of the region of small  $p_{\text{CR}}$ . To test the sensitivity of these results to the photon fragmentation function used, we repeat the calculation using the Kamae parametrization: We obtained a very similar photon spectral shape, as illustrated by the dashed green line in Fig. 9, though with a 20% higher flux. For an easier comparison of the shape, we normalize all the fluxes to coincide at 1 GeV. As we have shown above, the difference between the various fragmentation model manifest themselves mainly in the absolute photon yield, not in

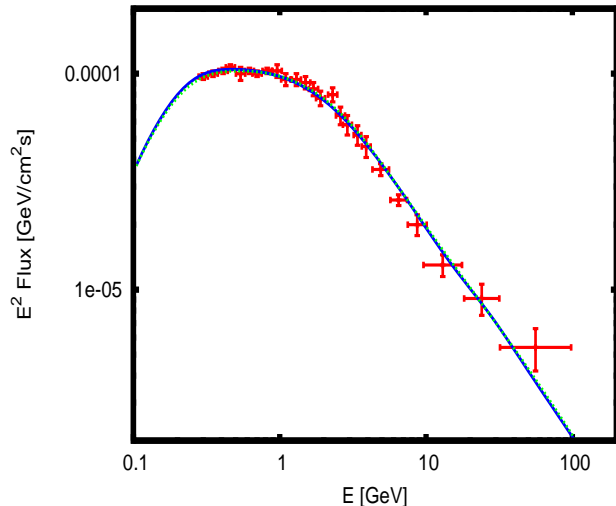


FIG. 9: Gamma-ray flux  $E^2\mathcal{F}(E)$  for a broken power-law with  $\beta_{\text{CR}} = -3$  for  $p_{\text{CR}} > 10$  GeV/c and  $\beta_{\text{CR}} = -2.4$  for  $p_{\text{CR}} < 10$  GeV/c as calculated using the combination of QGSJET-II and the ND model of Ref. [9] for  $E_{\text{thr}} = 50$  GeV (blue solid line) and based on the Kamae parametrization alone (green dashed line); All fluxes are normalized to coincide at 1 GeV. The gamma-ray spectrum derived in Ref. [32] from Fermi-LAT data is shown as points with error-bars.

the spectral shape.

Although the CR spectrum derived in Ref. [32] is consistent with the data, we consider it as less attractive: First, this solution requires additionally to the break at 9 GeV another one around 200 GeV, where the transition to the slope measured by PAMELA should take place. Second, both break energies have no obvious physical reason. In particular, it is surprising that the CR spectrum measured inside the Solar system differs substantially from the one of Galactic “sea” CRs up to 200 GeV. In contrast, the spectrum shown earlier in Fig. 8 has a single break at an energy where a change of the diffusion coefficient is expected [11, 20] and a single exponent  $\beta_{\text{CR}} = -2.85$  in agreement with PAMELA measurements.

#### IV. CONCLUSIONS

We have reconsidered the problem of determining the average properties of Galactic CRs using gamma-ray observations of molecular clouds. The largely improved quality of the observational data requires a careful treatment of the photon fragmentation function. Comparing photon fragmentation functions calculated in different approaches at high energies, we have argued that a combination of the Kamae parametrization and QGSJET-II provides the most reliable results. As our main result, we obtained that the spectral shape of CR protons as determined by PAMELA is consistent with the photon spectra

from molecular clouds observed by Fermi-LAT down to energies  $E \sim 1\text{--}2\text{ GeV}$ . The agreement is improved further, if the CR spectrum exhibits a break around 3 GeV. This gives additional evidence for a change of the diffusion coefficient around 3 GeV, which was previously suggested on theoretical grounds [20] and supported by observations [11].

### Acknowledgments

We would like to thank Andrii Neronov, Dima Semikoz, and Andrew Taylor for useful discussions, and Martin Pohl for comments on Ref. [13]. S.O. acknowledges the support of Norsk Forskningsradet within the program Romforskning.

*Note added:* After submission of this work, preprints by C. Dermer [arXiv:1206.2899] and by Malkov, Diamond, and Sagdeev [arXiv:1206.1384] appeared discussing also the connection of gamma-ray and CR spectra.

### Appendix A: Using the fragmentation functions

The photon fragmentation functions for proton-proton, proton-helium, and helium-proton collisions have been tabulated based on QGSJET-II simulations for a set of incident proton energies  $E_p$  between 10 and  $10^8$  GeV. For given energies of the primary  $E_p$  and secondary

$E_s$  particles the inclusive spectrum  $E_s d\sigma(E_p, E_s)/dE_s$  is then obtained via an interpolation between the tabulated values. In the case of pp collisions, the interpolation between the non-diffractive part of Kamae's parametrisation and QGSJET-II used in this work is provided. All procedures are available at <http://sourceforge.net/projects/ppfrag>.

### Appendix B: Comparison of the antiproton fragmentation function with data

In addition to photon production, we performed a comparison of model predictions for antiproton spectra in proton-proton collisions with available data, being motivated by the importance of those spectra in particular for dark matter searches.

As one can see from Figs. 10 and 11, pre-LHC data are somewhat uncertain concerning the antiproton yield in  $pp$  collisions, which partly explains the vast differences between various model predictions.

An important benchmark on the energy-dependence of the antiproton production is provided by the recent data obtained at LHC [33], as illustrated in Fig. 12. The antiproton yield in QGSJET-II-04 has been adjusted using these data.

Fragmentation functions for the production of antiprotons (plus antineutrons) in proton-proton, proton-helium, and helium-proton collisions are also available at <http://sourceforge.net/projects/ppfrag>.

- 
- [1] A. W. Strong, I. V. Moskalenko and V. S. Ptuskin, *Ann. Rev. Nucl. Part. Sci.* **57**, 285 (2007); for deviations from the standard diffusion picture see G. Giacinti, M. Kachelrieß and D. V. Semikoz, *Phys. Rev. Lett.* **108**, 261101 (2012).
  - [2] For a review see e.g. F.A. Aharonian, *Very high energy cosmic gamma radiation: a crucial window on the extreme Universe*, World Scientific Publishing, (River Edge, NJ, 2004).
  - [3] P. A. Caraveo *et al.*, *Astron. Astrophys.*, L3 (1980).
  - [4] S. W. Digel, S. D. Hunter, and R. Mukherjee, *Astrophys. J.* **441**, 270 (1995).
  - [5] S. W. Digel, E. Aprile, S. D. Hunter, R. Mukherjee, and F. Xu, *Astrophys. J.* **520**, 196 (1999).
  - [6] O. Adriani *et al.*, *Science* **332** (2011) 69.
  - [7] F. D. Aaron *et al.* (H1 Collaboration), *Eur. Phys. J. C* **71** (2011) 1771.
  - [8] O. Adriani *et al.*, *Phys. Lett. B* **703** (2011) 128.
  - [9] T. Kamae, N. Karlsson, T. Mizuno, T. Abe, T. Koi, *Astrophys. J.* **647** (2006) 692; Erratum-*ibid.* **662** (2007) 779; N. Karlsson and T. Kamae, *ibid.* **674** (2008) 278.
  - [10] S. R. Kelner and F. A. Aharonian, *Phys. Rev. D* **78** (2008) 034013; Erratum-*ibid.* **82** (2010) 099901.
  - [11] W. R. Webber and P. R. Higbie, *J. Geophys. Research* **113**, A11106 (2008).
  - [12] S. Ostapchenko, *Phys. Rev. D* **83** (2011) 014018.
  - [13] C.-Y. Huang, S.-E. Park, M. Pohl and C. D. Daniels, *Astropart. Phys.* **27**, 429 (2007).
  - [14] E.-J. Ahn *et al.*, *Phys. Rev. D* **80**, 094003 (2009).
  - [15] O. Adriani *et al.* [LHCf Collaboration], arXiv:1205.4578 [hep-ex].
  - [16] T. Kamae, T. Abe and T. Koi, *Astrophys. J.* **620** (2005) 244.
  - [17] A. B. Kaidalov, *Phys. Rep.* **50** (1979) 157.
  - [18] S. Ostapchenko, *Phys. Rev. D* **81** (2010) 114028.
  - [19] A. R. Bell, *Mon. Not. Roy. Soc.* **182**, 443 (1978).
  - [20] V. S. Ptuskin, I. V. Moskalenko, F. C. Jones, A. W. Strong and V. N. Zirakashvili, *Astrophys. J.* **642**, 902 (2006).
  - [21] K. Jaeger, D. Colley, L. Hyman, J. Rest, *Phys. Rev. D* **11** (1975) 2405.
  - [22] I. V. Ajinenko *et al.*, *Z. Phys. C* **35** (1987) 7.
  - [23] M. Aguilar-Benitez *et al.* (LEBC-EHS Collaboration), *Z. Phys. C* **50** (1991) 405.
  - [24] J. H. Campbell *et al.*, *Phys. Rev. D* **8** (1973) 3824; K. Jaeger *et al.*, *ibid.* **11** (1975) 1756.
  - [25] C. N. Booth *et al.*, *Phys. Rev. D* **27** (1983) 2018.
  - [26] B. Alper *et al.* (British-Scandinavian Collaboration), *Nucl. Phys. B* **100** (1975) 237.
  - [27] K. Guettler *et al.* (British-Scandinavian-MIT Collabora-



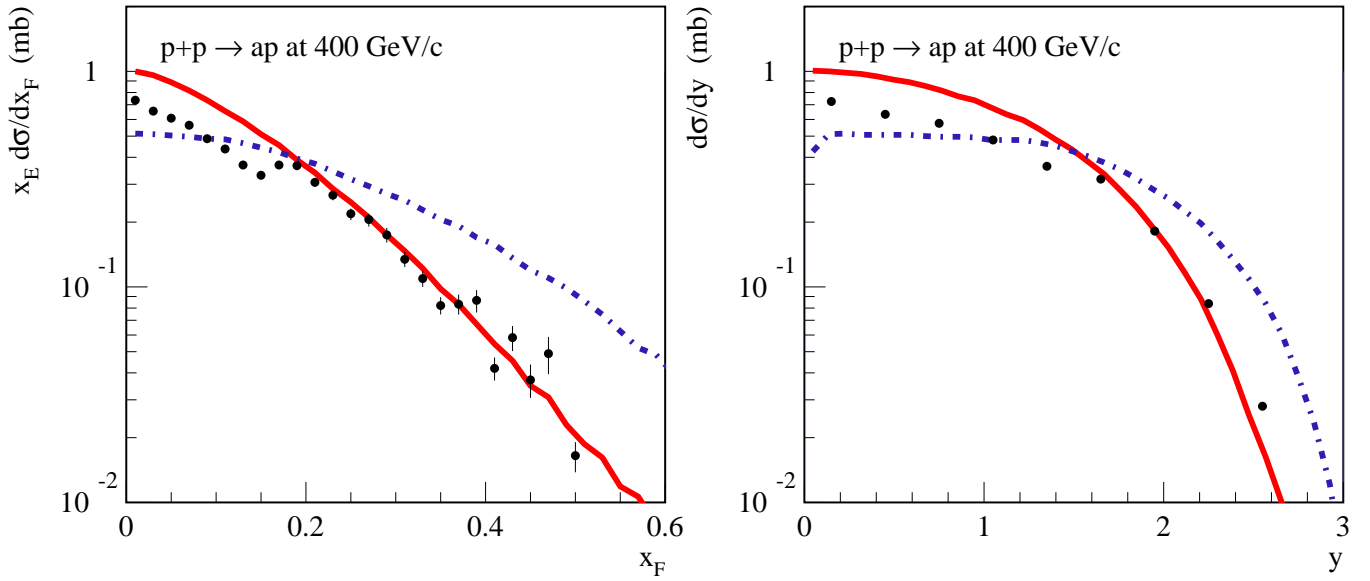


FIG. 10: Antiproton spectra in the c.m. frame for proton-proton collisions at 400 GeV/c: Feynman  $x$  spectrum (left), and rapidity distribution (right). Calculations with QGSJET-II-04 (red solid) and SIBYLL 2.1 (blue dot-dashed) are shown together with experimental data from Ref. [23].

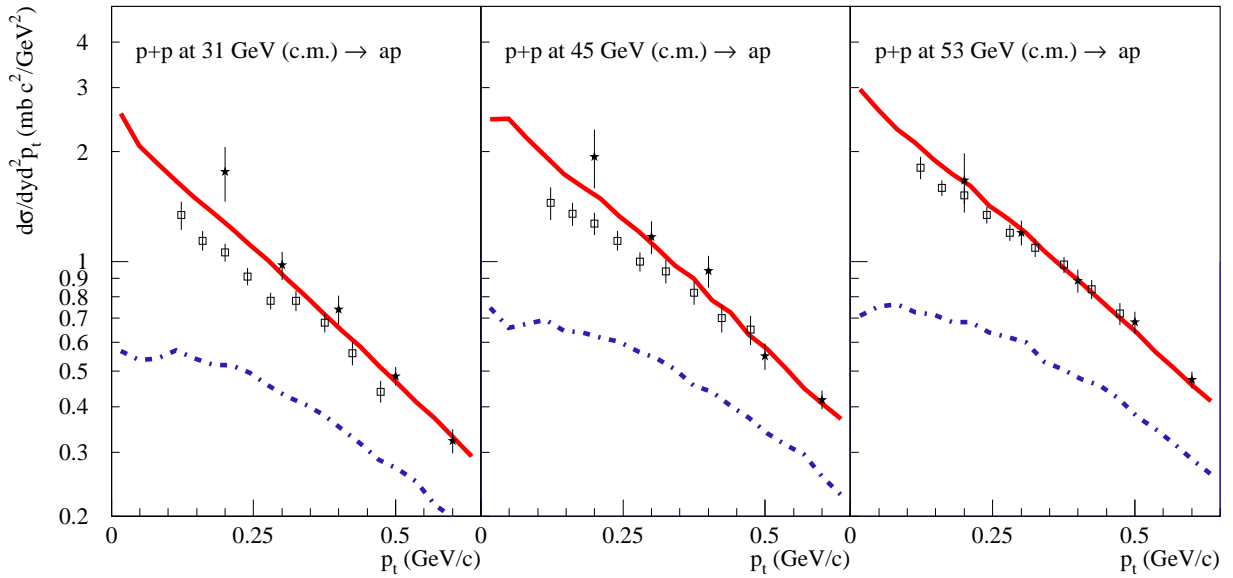


FIG. 11: Transverse momentum spectra of antiprotons at  $y = 0$  in the c.m. frame at  $\sqrt{s} = 31, 45,$  and  $53$  GeV, as calculated using QGSJET-II-04 (red solid) and SIBYLL 2.1 (blue dot-dashed) compared to experimental data from Refs. [26, 27].

tion), Nucl. Phys. B **116** (1976) 77.

- [28] M. Ackermann *et al.* [Fermi-LAT collaboration], *Astrophys. J.* **750**, 3 (2012).  
 [29] M. Ackermann *et al.* [Fermi-LAT collaboration], *Astrophys. J.* **726**, 81 (2011).  
 [30] A. A. Abdo *et al.* [Fermi-LAT collaboration], *Astrophys. J.* **703**, 1249 (2009).  
 [31] A. A. Abdo *et al.* [Fermi-LAT collaboration], *Phys. Rev.*

*Lett.* **103**, 251101 (2009), *ibid.* *Phys. Rev. Lett.* **104**, 101101 (2010), *Astrophys. J.* **710**, 133 (2010).

- [32] A. Neronov, D. V. Semikoz, A. M. Taylor, *Phys. Rev. Lett.* **108** (2012) 051105.  
 [33] K. Aamodt *et al.* (ALICE Collaboration), *Eur. Phys. J. C* **71** (2011) 1655; M. Chojnacki for the ALICE Collaboration, *J. Phys. G* **38** (2011) 124074.

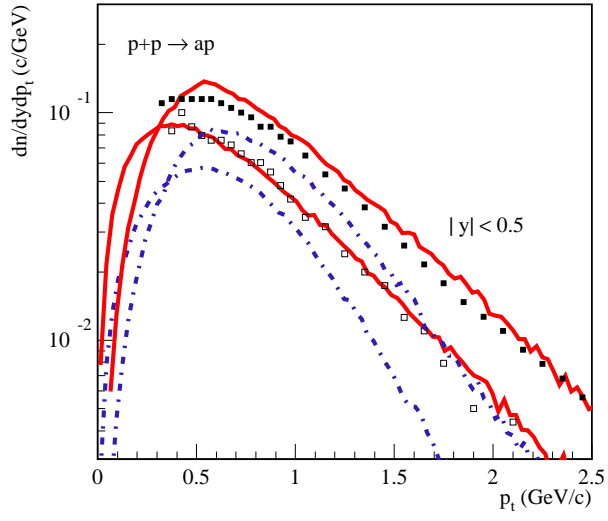


FIG. 12: Transverse momentum spectra of antiprotons at central rapidities ( $|y| < 0.5$ ) in the c.m. frame at  $\sqrt{s} = 900$  GeV (open squares) and 7 TeV (full squares) as measured by the ALICE Collaboration [33] compared to calculations with QGSJET-II-04 (red solid) and SIBYLL 2.1 (blue dot-dashed).